Jurnal Kejuruteraan 33(2) 2021: 229-238
https://doi.org/10.17576/jkukm-2021-33(2)-08

Forced Convective Heat Transfer Analysis for Two-dimensional Slot Jet of Water-CuO Nanofluid

Amin Etminan[a*] & Zambri Harun[b*]
[a]*Department of Mechanical Engineering, Memorial University of Newfoundland (MUN)*
St. John's, A1A 3X5, NL, Canada
[b]*Department of Mechanical and Manufacturing Engineering, Faculty of Engineering and Built Environment*
Universiti Kebangsaan Malaysia, 43600 Bangi, Malaysia

**Corresponding authors: aetminan@mun.ca & zambri@ukm.edu.my*

Received 26 September 2019, Received in revised form 01 September 2020
Accepted 15 September 2020, Available online 30 May 2021

ABSTRACT

This paper investigates the effect of the diameter and the volume fraction variation of the centre nanoparticles on the heat transfer characteristics of a two-dimensional slot jet. The jet impinges on stationary flat, convex, and concave aluminium plates. A forced convective heat transfer coefficient of water-CuO nanofluid impinges on a smooth plate under a constant heat flux. The finite volume method (FVM) is implemented for nanoparticles with diameters varying from 7 to 60 nanometers, volume fractions changing from 0 to 5%, and the Reynolds numbers ranging from 1800 to 2800. A grid independence study is carried out to find a grid size that predicts the results accurately and further grid refinement changes the results insignificantly. The single-phase model shows a capability to predicts the fluid and heat transfer parameters faster and make it more suitable for numerical simulations compared to the two-phase model. The results indicate a higher heat transfer coefficient of nanofluid in comparison with distilled water. As the Reynolds number and nanoparticle volume concentrations increase, the heat transfer rate increases on the surface whilst smaller nanoparticle diameters increase during the cooling process. The increase in the diameter of nanoparticles enhances the Nusselt number on the plate by up to 10%. The same geometrical details, thermophysical, and boundary conditions have been employed in all calculations for distilled water jet simulations to validate the fluid flow behaviour and heat transfer parameters with available experimental data in the literature.

Keywords: Heat Transfer; turbulent flow; slot jet; nanofluid; CuO nanoparticle

INTRODUCTION

In many industrial applications, jet impingement has been broadly utilized for the cooling of components exposed to high temperature or thermal flux because of its effectiveness in removing thermal energy (Liu & Lienhard 1993; Ghiti et al. 2013; Viskanta 1993; Lienhard & Hadeler 1999). In the last decade, many researchers have focused on enhancing heat transfer capabilities by using advanced technologies in many industries, including metal and glass annealing, paper drying, metal sheet manufacturing, turbine, and electronic chip cooling employ nanotechnology-level applications.

Several numerical and experimental studies (Martin 1977; Jambunathan et al. 1992; Zeitoun 2012) related to liquid impingement jets are available, which provides a database emphasizing the thermal advantages of different types of jet impingement on plates and their possible cooling abilities. A two-dimensional laminar flow slot jet impinging on a flat plate at different angles was theoretically analyzed (Garg & Jayaraj 1988). In that study, the conservation governing equations in primary variables were discretized using the finite difference method. The influence of the angle of impingement on the velocity and temperature profiles were studied. They revealed that the presence of a stagnation point when the impinging jet is oblique would affect the local Nusselt number, velocity distribution, and skin friction coefficient. Hofmann et al. 2007 experimentally focused on a pulsating impinging jet. The effect of the pulsation on the flow configuration and heat transfer characteristics were examined. They found a reduction of heat transfer at the stagnation point up to 50% with a large jet-to-plate distance. Comprehensive experimental research was done by Choi et al. 2000, determining the flow behaviour and heat transfer pattern of a cold jet impinging on a semi-circular concave plate over a wide range of the Reynolds numbers and jet-to-plate distances.

The hydrodynamics and heat transfer characteristics of the impingement jet, particularly the complexities of an oblique liquid plane jet, were numerically investigated by Tong 2003. In that research, the Navier-Stokes equations were solved employing an FVM on a fixed and non-uniform orthogonal mesh. Further, the effects of several parameters, including the Reynolds number, impingement angle, and inlet velocity profile, were examined. Ibuki et

al. 2009 experimentally investigated the characteristics of a convective heat transfer of a planar free water jet normally or obliquely impinging on a plate. In normal collisions, the Nusselt number was high along the impingement line and was reduced in the exit plane. The Nusselt number at the stagnation point was compared with several predictive correlations proposed by other researchers. Meanwhile, in oblique cases, the profile of the local Nusselt number was asymmetric.

The influence of the curvature of a plate on the convective heat transfer in the laminar confined jet was numerically studied (Tahsini & Tadayon Mousavi 2012). A two-dimensional, compressible jet was simulated by an FVM approach for three plate types, i.e., flat, concave, and convex plates. Their results showed that the Nusselt number at the stagnation point is highest on the convex and lowest on the concave plates. The experimental and numerical analysis of a water jet impingement on a convex, hemispherical plate was investigated (Hu & Zhang 2007). Their results proved that the Nusselt number of the flat plate is smaller than that of the convex plate.

A comprehensive review of liquid impingement jets and their features on convective heat transfer as well as several important correlations for Nusselt numbers were reviewed (Molana & Banooni 2013). Their review revealed that the Nusselt number increased when the Reynolds number and the volume concentration of nanoparticles increased. Meanwhile, using nanoparticles increased the pressure loss in the flow.

The capabilities of nanofluids when used in heat transfer processes involving liquid impingement jets were demonstrated by many researchers seeking to enhance the heat transfer coefficient of jets. The production of operational fluids with higher thermophysical properties–in particular, thermal conductivity–can be considered an efficient method for enhancing heat transfer. Numerous studies have demonstrated that using nanofluid is a state-of-the-art method for increasing the convective heat transfer coefficient of fluids. A cooling system involving an impingement jet of nanofluids can remove thermal energy generated by a heated surface faster in comparison to a distilled base-fluid, which was scrutinized later.

Gherasim et al. 2011 investigated the heat transfer enhancement abilities of a water-Al_2O_3 nanofluid as a coolant liquid inside a confined impinging jet. They demonstrated that the average Nusselt number increases with the nanoparticle volume fraction and the Reynolds number. It also decreased with an increase in the jet-to-plate distance. Naphon & Nakharintr 2012 studied the influence of the Reynolds number, inlet temperature, and heat flux on a convective heat transfer coefficient of water-TiO_2 nanofluid jet impingement on a rectangular, mini-fin heat sink. Their work indicated that the mean heat transfer coefficient for the nanofluid as a coolant liquid was higher than that for distilled water and that the corresponding mean temperature was 6.25% lower than the base fluid. Faris Abdullah et al. 2019 also found nanoparticle volume fraction and the Reynolds number dependency in their twin impingement jet of a heated aluminum plate using TiO_2.

Heat transfer removal from a moving isothermal hot surface under the attack of double impinging, vertical slot jets was numerically simulated by Başaran & Selimefendigil 2013; Ersayın & Selimefendigil 2013. Water-Al_2O_3 nanofluid with volumetric nanoparticle fractions ranging from 0 to 6% was used as the working fluid. The authors found that increasing the normalized plate velocity caused a rise in the heat transfer from the bottom surface. Likewise, increasing the Reynolds number of the slot jets removed heat from the surface faster. Furthermore, increasing the volumetric nanoparticle fraction contributed remarkably to the heat transfer enhancement. The turbulent flow and convective heat transfer of a confined, impinging, circular Al_2O_3 nanofluid jet on a heated flat plate, under constant heat flux, was numerically simulated by Huang & Jang 2013. Their results proved that the maximum Nusselt number occurred at the stagnation point and increased with the rise of nanoparticle volume concentration. Manca et al. 2011 carried out a numerical study on a laminar confined slot jet with water-Al_2O_3 nanofluid as its working fluid, impinging on a horizontal with a heated plate at a constant temperature. They showed that the heat transfer coefficient was increased with the rise in the nanoparticle effective density and the Reynolds numbers. Also, there was an increase of 32% in the average heat transfer coefficient for a nanoparticle with a volume fraction of 5%.

An experimental analysis of the heat transfer characteristics of the nanofluids using two different diameter sizes of the Cu nanoparticles suspended in water was investigated by Li et al. 2012. They observed a 52% rise in the convective heat transfer coefficient of the nanofluid with a 3% nanoparticle volume fraction in comparison to distilled water. Two comprehensive numerical simulations of laminar flow and forced convective heat transfer of water-Al_2O_3 and Ethylene Glycol-Al_2O_3 mixtures were thoroughly investigated by Maïga et al. 2004 & 2005 for two specific geometrical configurations, namely, a uniformly heated tube and a system of parallel, coaxial, and heated disks. They proved that the inclusion of nanoparticles into the base fluids produced remarkable growth in the heat transfer coefficient, enhanced with an increase of the nanoparticle volume fraction. In these studies, several correlations were obtained to compute the Nusselt number for the nanofluids, in terms of the Reynolds and the Prandtl numbers.

Yousefi et al. 2012 & 2013 carried out an experimental simulation of an impinging round jet on a circular disk and a planar jet on a V-shaped surface with water-Al_2O_3 nanofluid. Their experimental results showed an enhancement of the heat transfer coefficients at low nanofluid volume fractions. The authors studied a wide range of mean inlet velocity and impinging angles. Etminan et al. 2017 used CuO nanoparticles with different volume concentrations of 1% to 4% to enhance the rate of heat transfer in an equilateral triangular channel. They also found that the size of nanoparticles has an insignificant effect on heat transfer.

NUMERICAL SIMULATION AND BOUNDARY CONDITIONS

In the present study, an FVM approach is employed to analyze a nanofluid slot jet impingement on three flat, concave, and convex aluminum plates. There are two major advantages of an FVM, firstly, it enforces the conservation of quantities at a discretized level such as mass, momentum, energy remain conserved, and secondly takes full advantage of arbitrary meshes to approximate complex geometries (Kolditz 2002), which will help in our moderately complex geometry. A two-dimensional incompressible, Newtonian, and steady flow regime is considered for all simulations. For the Reynolds numbers of 1800, 2000, 2400, and 2800, the flow is found to be turbulent and the two-equation turbulent modeling is used. According to Figure 1, all geometrical details and boundary conditions are symmetrical, and only half of the computational domain is solved. A constant heat flux of 57693.3 W/m^2 is applied to the smooth and non-moving plates. The width of the planar jet is 1.6 mm, the length of the aluminum plate is 130 mm, and the distance between the jet and the plate is a constant value of 70 mm. A uniform velocity inlet flow is used for the jet and pressure outlet, and the adiabatic wall is employed on the left, right, and top boundaries of the computational domain. Uniform temperature distribution of 300 K is observed for the jet, and the shape of the CuO nanoparticles is considered spherical and uniform.

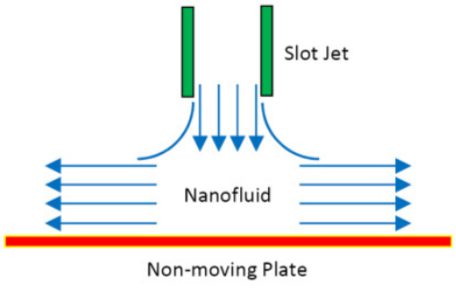

FIGURE 1. Two-dimensional schematic of the problem under consideration.

NUMERICAL PROCEDURE VALIDATION

The numerical modeling and solution procedure of the present study is validated by experimental data provided by Baydar (1999) and Gulati et al. (2009) for both fluid flow and heat transfer global parameters (Figures 2 and 3). Numerical setup, including geometrical details and boundary conditions, is compared to the results presented by Baydar (1999) and Gulati et al. (2009). The pressure coefficient distribution on the flat plate along the horizontal X-axis is in agreement with the experimental data, this can be seen in Figure 2. As is also shown in Figure 2, the highest value of Cp occurs at the stagnation point opposite the slot jet. Further, the average Nusselt number distribution on the plate is illustrated in Figure 3. As can be observed, there is just a small difference between the provided numerical results and the experimental data. This can be attributed to the numerical discretization method, the Reynolds stress tensors, and scalar heat flux modellings. The highest deviation appears where the flow direction is suddenly changed to the lateral sides of the plate.

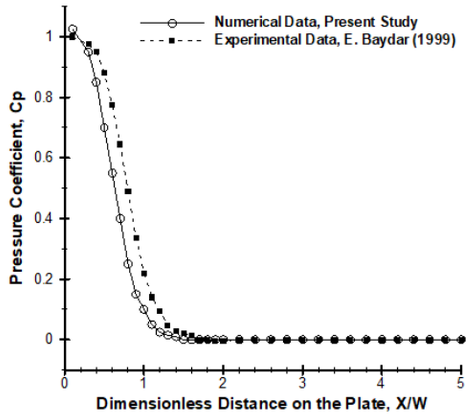

FIGURE 2. Pressure coefficient distribution at the impingement surface for Re=5000 and H/W=1 for distilled water jet.

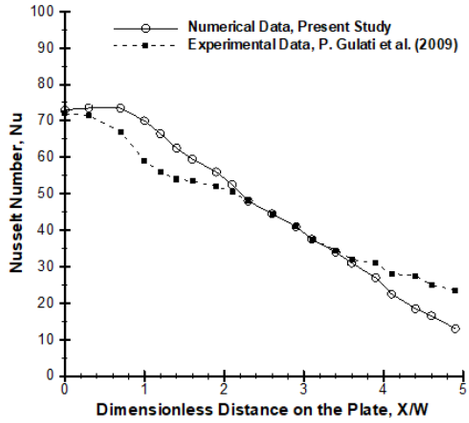

FIGURE 3. Nusselt number distribution at the impingement surface for Re=5000 and H/W=1 for distilled water.

GRID INDEPENDENCE

A mesh study is performed to ascertain an optimal number of grids and the influence of the number of cells on the heat transfer and pressure coefficients. Four non-uniform cases of mesh, 15800, 18700, 22800, and 24375 cells, are provided to determine an independent grid number, where the smallest cell size is equal by 0.2 mm adjacent to the solid surfaces. Local Nusselt number distribution on the heated flat plate is illustrated in Figure 4 for the Reynolds number of 1800. The simulations indicate that there is a negligible deviation between the provided results for grid numbers of 22800 and 24375. Therefore, the grid number of 22800 was selected to minimize the computational time for all the following simulations.

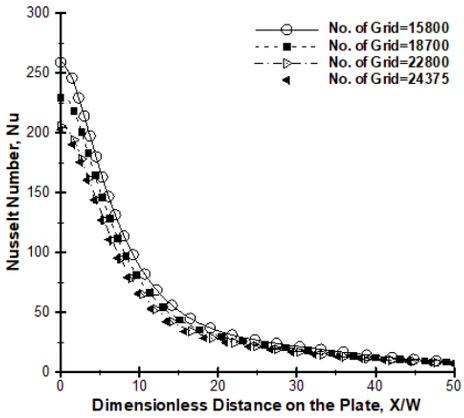

FIGURE 4. Analysis of grid independence by Nusselt number at the flat impingement surface.

GOVERNING EQUATIONS AND NUMERICAL SOLUTION METHOD

Equations governing a two-dimensional, incompressible, and steady turbulent flow and heat transfer of the water-CuO nanofluid, including continuity, momentum, and energy equations, are shown as equations (1) to (3). The finite volume solution method has been utilized for solving the governing equations in the Cartesian coordinate system.

$$\frac{\partial\left(\rho u_i\right)}{\partial x_i}=0 \tag{1}$$

$$\frac{\partial\left(\rho u_i u_j\right)}{\partial x_j}=-\frac{\partial P}{\partial x_i}+\frac{\partial}{\partial x_j}\left[\mu\left(2S_{ij}\right)-\rho\overline{u_i' u_i'}\right] \tag{2}$$

$$\frac{\partial\left(\rho u_i T\right)}{\partial x_j}=\frac{\partial}{\partial x_j}\left[\frac{\mu}{Pr}\frac{\partial T}{\partial x_i}-\rho\overline{u_i' T'}\right] \tag{3}$$

The Semi-Implicit Method for Pressure Linked Equations Consistent (SIMPLEC) algorithm solves velocity-pressure coupled equations (Versteeg & Malalasekera 2007), which were used by Etminan et al. 2018 to simulate the heat transfer and vortex shedding from bluff bodies in an external flow. The remainder of 10^{-6} also achieves exact results and negligible errors from the present problem solving, and optimizes computer memory usage in the numerical simulation process.

Both algebraic terms $\overline{u_i' T'}$ and $\overline{u_i' u_i'}$, namely, the Reynolds stress tensor and turbulent heat flux vector, must be numerically modelled. According to Sharif & Mothe 2009, the turbulent model k-ε RNG calculated more accurate results as well as more rates of convergence than the stress tensor. They showed that this model, when compared with other turbulent models, has a higher success rate for predicting flow and thermal characteristics of an impingement jet on a concave plate. The most useful model for the scalar term $\overline{u_i' T'}$ is the Simple Eddy Diffusivity (SED) model proposed by Daly & Harlow 1970:

$$\overline{u_i' T'}=-\frac{\nu_t}{Pr_t}\frac{\partial T}{\partial x_i} \tag{4}$$

where Pr_t is considered the constant value of 0.85, (Daly & Harlow 1970). The turbulent model k-ε RNG equations are as follows (Sharif & Mothe 2009):

$$\frac{\partial\left(\rho k u_i\right)}{\partial x_i}=\frac{\partial}{\partial x_j}\left[\left(\mu+\frac{\mu_t}{\sigma_k}\right)\frac{\partial k}{\partial x_j}\right]+P_k-\rho\varepsilon \tag{5}$$

$$\frac{\partial\left(\rho\varepsilon u_i\right)}{\partial x_i}=\frac{\partial}{\partial x_j}\left[\left(\mu+\frac{\mu_t}{\sigma_\varepsilon}\right)\frac{\partial\varepsilon}{\partial x_i}\right]+C_{1\varepsilon}\frac{\varepsilon}{k}P_k$$

$$-C_{2\varepsilon}\rho\frac{\varepsilon^2}{k}-\frac{C_\mu\eta^3\left(1-\frac{\eta}{\eta_0}\right)}{1+\beta\eta^3}\frac{\varepsilon^2}{k} \tag{6}$$

where,

$$P_k=\left[2\mu_t S_{ij}-\frac{2}{3}\rho k S_{ij}\right]\frac{\partial u_j}{\partial x_i} \tag{7}$$

$$\eta=\frac{Sk}{\varepsilon} \tag{8}$$

$$S=\sqrt{2S_{ij}S_{ij}} \tag{9}$$

$$S_{ij}=0.5\left[\frac{\partial u_i}{\partial x_j}+\frac{\partial u_j}{\partial x_i}\right] \tag{10}$$

where the constant values in equations above are as follows:

$$C_{1\varepsilon}=1.42,\ C_{2\varepsilon}=1.68,\ C_\mu=0.0845,$$

$$\sigma_k=\sigma_\varepsilon=0.7194,\ \beta=0.012,\ \eta_0=4.38$$

The thermo-physical properties of the distilled water, CuO nanoparticles, and nanofluid are written in Table 1. For computing nanofluid density, the equation proposed by

Aminossadati & Ghasemi 2009; Malvandi & Ganji 2014; Mahdy 2012 is used and is shown as follows:

$$\rho_{nf} = (1-\varphi)\rho_f + \varphi\rho_p \tag{11}$$

where parameters ρ_{nf}, ρ_f, φ and ρ_p refer to the nanofluids density, base fluid density, the volume fraction of solid nanoparticles, and solid nanoparticle density, respectively.

The effective heat distribution coefficient of the nanofluid is calculated from the following formula (Karimipour et al. 2014):

$$\alpha_{eff,nf} = \frac{k_{eff}}{\rho_{nf} C_{p,nf}} \tag{12}$$

where α_{eff}, C_{pnf}, ρ_{nf} and k_{eff} are thermal diffusivity, specific heat capacity, density, and effective thermal conductivity of nanofluids, respectively. Specific heat capacity of the nanofluid is calculated by the following formula [39]:

$$(\rho C_p)_{nf} = (1-\varphi)(\rho C_p)_f + \varphi(\rho C_p)_p \tag{13}$$

The Brinkman relationship is used to calculate the effective dynamic viscosity of nanofluid (Brinkman 1952; Karimipour et al. 2015):

$$\mu_{nf} = \frac{\mu_f}{(1-\varphi)^{2.5}} \tag{14}$$

where μ_{nf} and μ_f are the dynamic viscosity of fluid and nanofluids, respectively. To calculate the effective thermal conductive coefficient of nanofluid for suspensions having sphere-like particles, the relationship provided by Patel et al. 2005 is used:

$$k_{eff} = k_f \left[1 + \frac{k_p A_p}{k_f A_f} + c k_p Pe \frac{A_p}{k_f A_f} \right] \tag{15}$$

where the experimental constant is c=36000 and terms k_f, k_p, and Pe refer to the thermal conductivity of the base fluid, solid nanoparticles, and the Peclet number, respectively. The rest terms in equation (15) can be obtained using the following equations Patel et al. 2005:

$$\frac{A_p}{A_f} = \frac{d_f}{d_p}\frac{\varphi}{1-\varphi} \tag{16}$$

$$Pe = \frac{u_s d_p}{\alpha_f} \tag{17}$$

where the water molecule diameter equals d_f = 2Å, the CuO nanoparticle molecule diameter varies between 7 nm and 60 nm, and the u_s value is the Brownian motion velocity of nanoparticles and is calculated by the following formula (Goodarzi et al. 2014):

$$u_s = \frac{2\kappa_b T}{\pi \mu_f d_p^2} \tag{18}$$

where, κ_b = 1/3807 × 10^{-23} J/K value is the Boltzmann constant. For calculating the local Nusselt number along the microchannel walls, the following equation is used, where the values of T_w and T_m are the average temperatures of the wall and bulk fluid, respectively, and q'' is the heat flux applied to the aluminum plate (Xia et al. 2013):

$$\mathrm{Nu}_{ave.} = \frac{q'' W}{k_f (T_w - T_m)} \tag{19}$$

RESULTS AND DISCUSSION

First of all, a comparison between single- and two-phase models is carried out as is illustrated in Figure 5. Figure 5 shows that both models are able to predict the Nusselt number distribution along the width of the surface. However, the single-phase model underestimates the amount of the Nusselt number and the differences in some areas along the

TABLE 1. Thermophysical properties of the nanofluid and solid nanoparticles (Mahdy 2012).

Distilled Water		Nanoparticle CuO	Nanofluid				
			φ=1%	φ=2%	φ=3%	φ=4%	φ=5%
ρ (kg/m^3)	998.2	8933	1077.6	1156.9	1236.2	1315.6	1394.9
C_p *(J/kgK)*	4182	385	3867.2	3595.6	3358.9	3150.7	2966.2
k (W/m K)	0.6130	400	0.6315	0.6504	0.6696	0.6893	0.7094
μ (Pa s)	0.00103	-----	0.00108	0.001198	0.001333	0.001493	0.001677
Pr	6.8426	-----	6.6662	6.6275	6.6897	6.8255	7.0144

width of the plate, reaching around 15-20%. Based on the provided data by Maïga et al. 2004 & 2005, the single-phase model evaluates the thermal and fluid parameters faster in comparison to the two-phase model, with acceptable accuracy when the nanoparticle diameters are smaller than 100 nm and the concentration is less than 6%. Therefore, in the following sections, the single-phase model is employed for all simulations.

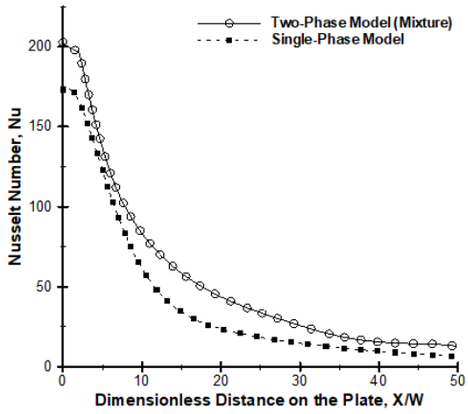

FIGURE 5. Nusselt number distribution at flat impingement surface of single phase and mixture models; d=7 nm, Re=1800, and φ=2%.

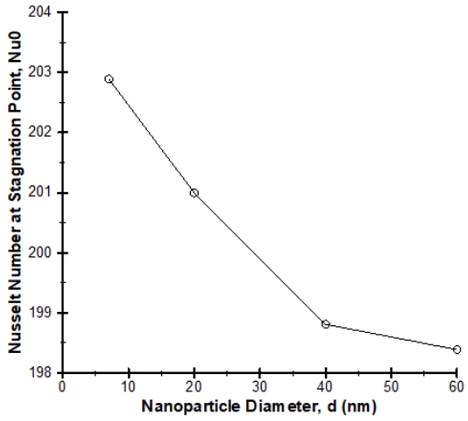

FIGURE 6. Local Nusselt number at stagnation point of flat impingement plate; Re=1800, and φ=2%.

Figure 6 shows the variation of the value of the Nusselt number at the stagnation point versus the nanoparticles diameter. The inverse relationship is evident from the graph where the rise in nanoparticle diameter leads to a decrease in the Nusselt number at the stagnation point. Furthermore, it can be concluded that the critical nanoparticle size acting on the Nusselt number at the stagnation point can be set as 40-50 nm. An increase in the nanoparticle diameter to a number higher than the critical number leads to very small changes in the value of the Nusselt number at the stagnation point. It should be noted that the peak value of the Nusselt number is related to the smallest nanoparticle diameter, leading to higher Nusselt numbers.

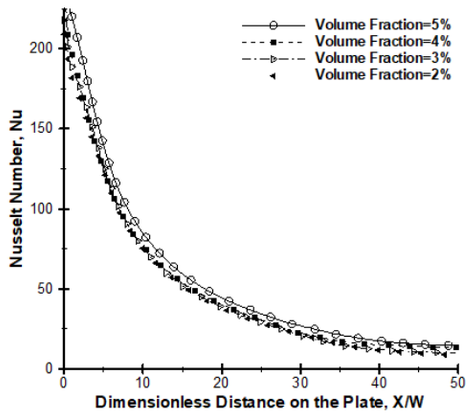

FIGURE 7. Nusselt number distribution at flat impingement plate; Re=1800, and d=7 nm.

Figure 7 illustrates the distribution of the Nusselt number along with the width of the impingement surface for different volume fractions. Thus, the effect of volume fraction on the value of the Nusselt number is low for a small range of volume concentration. As the volume fraction increases, the magnitude of the Nusselt number increases as well. Based on Figure 7, the 5% volume fraction causes an observable increase in the Nusselt number in comparison with other simulated volume fractions; however, this increase of magnitude is insignificant.

As indicated in Figure 8, it is clear that the increase in the mean jet velocity causes a significant effect on the distribution of the Nusselt number. When the high-velocity jet vertically impinges on a surface, thin hydrodynamic and thermal boundary layers are formed at the stagnation point, developing outward over time. Based on the amount of the Prandtl number, which is greater than 1, the hydrodynamic boundary layer is thicker than the thermal boundary layer. The temperature at the stagnation zone is low and increases outward, which this process leads to the peak value of the Nusselt number at the impingement point of the stagnation region. As is shown in Figure 8, higher jet velocity can increase the Nusselt number up to 50% higher.

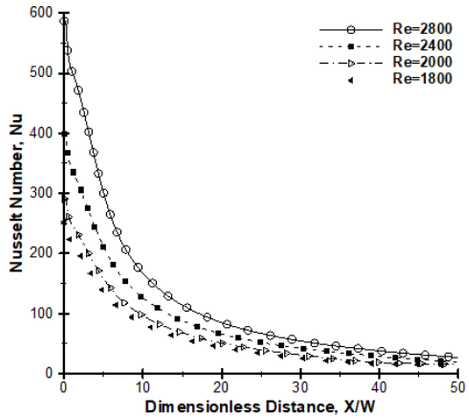

FIGURE 8. Nusselt number distribution at flat impingement plate; d=7 nm, and φ=5%.

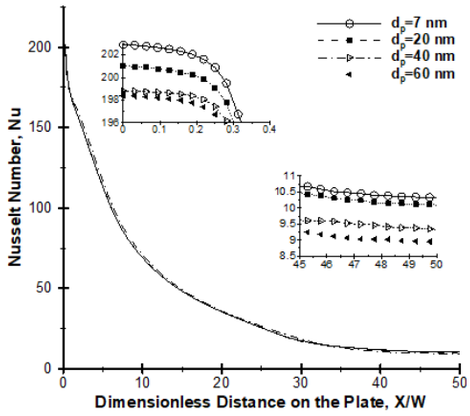

FIGURE 9. Nusselt number distribution at flat impingement plate and two selected zoomed-out areas for several nanoparticle diameters; Re=1800, and φ=2%.

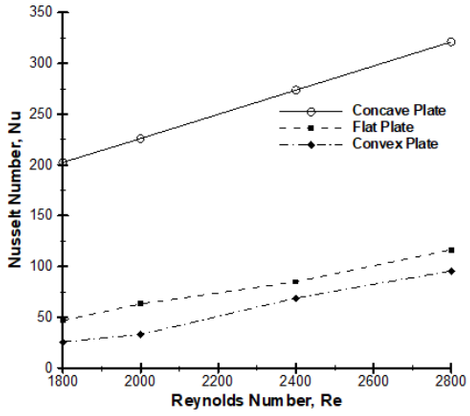

FIGURE 10. Local Nusselt number at stagnation point for d=7 nm, and φ=2%.

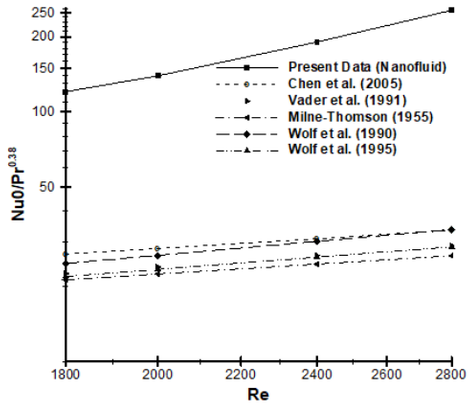

FIGURE 11. Comparison between the current results of the stagnation Nusselt number for normal impingement with previously documented correlations for impingement with distilled water.

Figure 9 illustrates the effect of different nanoparticle diameters on the distribution of the Nusselt number, along with the width of the impingement surface. Based on this figure, the effect of nanoparticle diameters at the stagnation zone is about 1%; however, at the further distance from the stagnation zone, the effect of the nanoparticles increases by up to 10%. This can be described as a value of the Nusselt number. Since the value of the Nusselt number is high at the stagnation point, the nanoparticle diameter does not play a significant role; however, away from this zone, the nanoparticle diameter becomes a significant factor. This is because of the drastic drop in the Nusselt number (about 90%).

Impingement on the different types of surfaces affects the magnitude of the Nusselt number which this is better explained as a change in the hydrodynamic and thermal boundary layers. A change of surface to a concave plate notably increases the highest Nusselt number in comparison with the flat and the convex plates. Further, the convex shape of the plate reduces the maximum Nusselt number as well.

Figure 10 depicts the Nusselt number for all three types of plates versus the value of the Reynolds number. Regarding the earlier-mentioned argument, the high velocity of the inlet jet, which causes a high Reynolds number, leads to an increase of the Nusselt number. Figure 11 shows numerical data of the present study for water-CuO nanofluid with a nanoparticle diameter of 7 nm and a volume fraction of 5% with the solid line. Some other theoretical formulas proposed by authors available in the literature are illustrated in this figure for distilled water with different Reynolds number ranges for comparison with the current results. As seen, there is a huge deviation of the stagnation Nusselt number between the impingement containing nanoparticles, with the output of correlations for the impingement with water.

CONCLUSION

Numerical simulation of the heat transfer characteristics of a two-dimensional slot jet impingement on a plate is performed. The effect of several parameters, such as the nanoparticles diameter and their volume fraction as well as the influence of the impingement plate shape on the heat transfer coefficient were discussed and analyzed.

A precise grid independence study was carried out to discover an optimal number of the grids, and the grid resolution was improved to evaluate the proper truncation error and increase the accuracy of the numerical simulation.

Sensitivity analysis regarding the effect of the volume fraction on the Nusselt number showed that the volume concentration does not affect the

Nusselt number and there is a low dependency. As the volume fraction starts to grow, the magnitude of the Nusselt number increases. The results of a simulation demonstrated that an increase in the mean jet velocity, which causes an increase in the value of the Reynolds number, significantly affects the distribution of the Nusselt number. Furthermore, due to the high Nusselt number, the dependency of the Nusselt number on the nanoparticles diameter is low near to the stagnation point. However, the dependency of the Nusselt number on the nanoparticles diameter increases at

the far edge of the plate, due to the high reduction of the Nusselt number.

Additionally, jet impingement on the different types of plates affects the Nusselt number, which can be considered as a result of a change in the hydrodynamic and thermal boundary on these surfaces. A change of surface to a concave shape extremely increases the highest value of the Nusselt number; however, the convex shape reduces the maximum Nusselt number.

NOMENCLATURE

C	experimental constant, 36000
C_p	pressure coefficient
C_{np}	specific heat capacity, J/kg.K
d	nozzle diameter, m
d_p	nanoparticles diameter
d_f	base fluid molecule diameter
H	the vertical jet-to-surface distance, m
k	turbulent kinetic energy
K	thermal conductivity coefficient, W/m.K
k_f	thermal conductivity coefficient of the base fluid, W/m.K
k_p	thermal conductivity coefficient of nanoparticles, W/m.K
Nu	Nusselt number
Nu_0	Nusselt number at the stagnation point
P	pressure, Pa
Pe	Peclet number
Pr	Prandtl number
R	radial distance measured from the stagnation point, m
Re	Reynolds number
T	temperature, K
T_m	bulk temperature of the fluid, K
T_w	averaged temperature of the wall, K
q''	heat flux, W/m^2
u	velocity component along X, m/s
u_s	exit velocity of the jet, m/s
W	width of the jet
x	cartesian coordinate axis
X	horizontal coordinate axis along the impingement surface

Subscript

0	parameters at stagnation point
ave.	averaged
eff	effective
f	fluid
i	axis along the horizontal direction of the impingement surface
j	axis along the vertical direction on impingement surface
k	turbulent kinetic energy
m	mean
nf	nanofluid
p	solid nanoparticles
ε	dissipation rate of turbulent kinetic energy
1ε	first constant value in ε equation
2ε	second constant value in ε equation

Greek symbols

α	thermal diffusivity
β	thermal expansion coefficient, 1/K
ε	dissipation rate of turbulent kinetic energy, m^2/s^3
κ_b	Boltzmann constant, 1.3807×10^{-23} J/K
μ	dynamic viscosity, Pa.s
υ	kinematics viscosity, m^2/s
ρ	density, kg/m^3
φ	volume fraction of nanoparticles
∂	partial differential operator

ACKNOWLEDGEMENTS

The research has been funded by the Ministry of Science, Technology, and Innovation of Malaysia under science fund grant SF1326 and UKM grant GUP-2018-102.

DECLARATION OF COMPETING INTEREST

None.

REFERENCES

Aminossadati, S.M. & Ghasemi, B. 2009. Natural convection cooling of a localized heat source at the bottom of a nanofluid-filled enclosure, *European Journal of Mechanics-B/Fluids* 28(5): 630-640.

Başaran, A. & Selimefendigil, F. 2013. Numerical study of heat transfers due to twinjets impingement onto an isothermal moving plate, *Mathematical and Computational Applications* 18(3): 340-350.

Baydar, E. 1999. Confined impinging air jet at low Reynolds numbers, *Experimental Thermal and Fluid Science* 19(1): 27-33.

Brinkman, H.C. 1952. The viscosity of concentrated suspensions and solutions, *The Journal of Chemical Physics* 20: 571-581.

Chen, Y.C., Ma, C.F., Qin, M. & Li, Y.X. 2005. Theoretical study on impingement heat transfer with single-phase free-surface slot jets, *International Journal of Heat and Mass Transfer* 48: 3381-3386.

Choi, M., Yoo, H.S., Yang, G., Lee, J.S. & Sohn, D.K. 2000. Measurement of impinging jet flow and heat transfer on a semi-circular concave surface, *International Journal of Heat and Mass Transfer* 43(10): 1811-1822.

Daly, B.J. & Harlow, F.H. 1970. Transport equation in turbulence. *Physics of Fluids* 13: 2634-2649.

Ersayın, E. & Selimefendigil, F. 2013. Numerical investigation of impinging jets with nanofluids on a moving plate. *Mathematical and Computational Applications* 18(3): 428-437.

Etminan, A., Harun, Z. & Sharifian, A. 2017. Numerical Investigation of Nanofluid Laminar Forced Convective Heat Transfer inside an Equilateral Triangular Tube. *IOP Conference Series: Earth and Environmental Science* 51: 1-6.

Etminan, A., Sharifian, A., Reda, E. & Harun, Z. 2018. Time-averaged heat transfer and vortex shedding of a singular and twin heated bluff bodies in cross flow. *International Journal of Engineering and Technology* 7: 270-276.

Faris Abdullah, M., Zulkifli, R., Harun, Z., Abdullah, S., Wan Ghopa, W.A., Soheil Najm, A. & Humam Sulaiman, N. 2019. Impact of the TiO2 nanosolution concentration on heat transfer enhancement of the twin impingement jet of a heated aluminum plate. *Micromachines* 10(3):176.

Garg, V.K. & Jayaraj, S. 1988. Boundary layer analysis for two-dimensional slot jet impingement on inclined plates. *Journal of Heat Transfer* 110(3): 577-582.

Gherasim, I., Roy, G., Nguyen, C.T. & Vo-Ngoc, D. 2011. Heat transfer enhancement and pumping power in confined radial flows using nanoparticle suspensions (nanofluids). *International Journal of Thermal Sciences* 50(3): 369-377.

Ghiti, N., Bentebbiche, A.A. & Hanchi, S. 2013. Numerical study of multi-fuel jet inverse diffusion flame. *American Journal of Mechanical Engineering* 1(4): 76-81.

Goodarzi, M., Safaei, M.R., Vafai, K., Ahmadi, G., Dahari, M., Kazi, S.N. & Jomhari, N. 2014. Investigation of nanofluid mixed convection in a shallow cavity using a two-phase mixture model. *International Journal of Thermal Sciences* 75: 204-220.

Gulati, P., Katti, V. & Prabhu, S.V. 2009. Influence of the shape of the nozzle on local heat transfer distribution between the smooth flat surface and impinging air jet. *International Journal of Thermal Sciences* 48(3): 602-617.

Hofmann, H.M., Movileanu, D.L., Kind, M. & Martin, H. 2007. Influence of a pulsation on heat transfer and flow structure in submerged impinging jets. *International Journal of Heat and Mass Transfer* 50(17-18): 3638-3648.

Hu, G. & Zhang, L. 2007. Experimental and numerical study on heat transfer with impinging circular jet on a convex hemispherical surface. *Heat Transfer Engineering* 28(12): 1008-1016.

Huang, J.B. & Jang, J.Y. 2013. Numerical study of a confined axisymmetric jet impingement heat transfers with nanofluids. *Scientific Research ENG* 5: 69-74.

Ibuki, K., Umeda, T., Fujimoto, H. & Takuda, H. 2009. Heat transfer characteristics of a planar water jet impinging normally or obliquely on a flat surface at relatively low Reynolds numbers. *Experimental Thermal and Fluid Science* 33(8): 1226-1234.

Jambunathan, K., Lai, E., Moss, M.A. & Button, B.L. 1992. A review of heat transfer data for single circular jet impingement. *International Journal of Heat and Fluid Flow* 13(2): 106-115.

Karimipour, A., Hossein Nezhad, A., D'Orazio, A., Hemmat Esfe, M., Safaei, M.R. & Shirani, E. 2015. Simulation of copper–water nanofluid in a microchannel in slip flow regime using the lattice Boltzmann method. *European Journal of Mechanics-B/ Fluids* 49(A): 89-99.

Karimipour, A., Hemmat Esfe, M., Safaei, M.R., Toghraie, D., Jafari, S. & Kazi, S.N. 2014. Mixed convection of a copper-water nanofluid in a shallow inclined lid-driven cavity using lattice Boltzmann method. *Physica A: Statistical Mechanics and Its Applications* 402: 150-168.

Kolditz, O. 2002. Finite volume method. In *Computational Methods in Environmental Fluid Mechanics*. Springer, Berlin, Heidelberg. https://doi.org/10.1007/978-3-662-04761-3_8

Li, Q., Xuan, Y. & Yu, F. 2012. Experimental investigation of submerged single jet impingement using Cu-water nanofluid. *Applied Thermal Engineering* 36: 426-433.

Lienhard, J.H. & Hadeler, J. 1999. High heat flux cooling by liquid jet-array modules, *Chemical Engineering Technology*, 22(11): 967-970.

Liu, X. & Lienhard, J. 1993. Extremely High Heat Fluxes Beneath Impinging Liquid Jets, Journal of Heat Transfer, 115(2): 472-476.

Mahdy, A. 2012. Unsteady mixed convection boundary layer flow and heat transfer of nanofluids due to stretching sheet, *Nuclear Engineering, and Design*, 249: 248-255.

Maïga, S.E.B., Nguyen, C.T., Galanis, N. & Roy, G. 2004. Heat transfer behaviors of nanofluids in a uniformly heated tube, *Superlattices Microstructures*, 35(3-6): 543-557.

Maïga, S.E.B., Palm, S.J., Nguyen, C.T., Roy, G. & Galanis, N. 2005. Heat transfer enhancement by using nanofluids in forced convection flows, *International Journal of Heat and Fluid Flow*, 26(4): 530-546.

Malvandi, A. & Ganji, D.D. 2014. Magnetohydrodynamic mixed convective flow of Al2O3-water nanofluid inside a vertical microtube, *Journal of Magnetism and Magnetic Materials*, 369: 132-141.

Manca, O., Mesolella, P., Nardini, S. & Ricci, D. 2011. Numerical study of laminar confined impinging slot Jets with nanofluids, *Nanoscale Research Letters*, 6(1): 188-204.

Martin, H. 1977. Heat and mass transfer between impinging gas jets and solid surfaces, *Advances in Heat Transfer*, 13: 1-60.

Milne-Thomson, L.M. 1960. Theoretical Hydrodynamics, 4th ed., Macmillan & Co., New York, 279-289.

Molana, M. & Banooni, S. 2013. Investigation of heat transfer processes involved liquid impingement jets: a review, *Brazilian Journal of Chemical Engineering*, 30(3): 413-435.

Naphon, P. & Nakharintr, L. 2012. Nanofluid jet impingement heat transfer characteristics in the rectangular mini-fin heat sink, *Journal of Engineering Physics and Thermophysics*, 85(6): 1432-1440.

Patel, H.E., Sundararajan, T., Pradeep, T., Dasgupta, A., Dasgupta, N. & Das, S.K. 2005. A micro-convection model for thermal conductivity of nanofluids, *Pramana Journal of Physics*, 65(5): 863-869.

Sharif, M.A.R. & Mothe, K.K. 2009. Evaluation of Turbulence Models in the Prediction of Heat Transfer Due to Slot Jet Impingement on Plane and Concave Surfaces, *Numerical Heat Transfer, Part B: Fundamentals*, 55(4): 273-294.

Tahsini, A.M. & Tadayon Mousavi, S. 2012. Laminar impinging jet heat transfer for curved plates. *International Journal of Mechanical, Aerospace, Industrial, Mechatronic and Manufacturing Engineering* 6(12): 2788-2793.

Togun, H., Safaei M.R., Sadri, R., Kazi, S.N., Badarudin, A., Hooman, K. & Sadeghinezhad, E. 2014. Numerical simulation of laminar to turbulent nanofluid flow and heat transfer over a

backward-facing step. *Applied Mathematics, and Computation* 239: 153-170.

Tong, A.Y. 2003. On the impingement heat transfer of an oblique free surface plane jet. *International Journal of Heat and Mass Transfer* 46(11): 2077-2085.

Vader, D.T., Incropera, F.P. & Viskanta, R. 1991. Local convective heat transfers from a heated surface to an impinging, planar jet of water. *International Journal of Heat and Mass Transfer* 34(3): 611-623.

Versteeg, H.K. & Malalasekera, W. 2007. *An Introduction to Computational Fluid Dynamics-The Finite Volume Method*. 2nd edition. Pearson Education Limited.

Viskanta, R. 1993. Heat transfer to impinging isothermal gas and flame jets. *Experimental Thermal and Fluid Science* 6(2): 111-134.

Wolf, D.H., Viskanta, R. & Incropera, F.P. 1990. Local convective heat transfer from a heated surface to a planar jet of water with a non-uniform velocity profile. *ASME Journal of Heat Transfer* 112: 899-905.

Wolf, D.H., Viskanta, R. & Incropera, F.P. 1995. Turbulence dissipation in a free-surface jet of water and its effect on local impingement heat transfer from a heated surface part 1-flow structure. *ASME Journal of Heat Transfer* 117: 85-94.

Xia, G., Zhai, Y. & Cui, Z. 2013. Numerical investigation of thermal enhancement in a micro heat sink with fan-shaped reentrant cavities and internal ribs. *Applied Thermal Engineering* 58(1-2): 52–60.

Yousefi, T., Mahdavi, R. & Paknezhad, M. 2012. Slot jet of Al2O3-water nanofluid on a flat plate, *In ICTEA conference*, Turkey.

Yousefi, T., Shojaeizadeh, E., Mirbagheri, H.R., Farahbaksh, B. & Saghir, M.Z. 2013. An Experimental investigation on impingement of a planar jet of Al2O3-water nanofluid on a V-shaped plate. *Experimental Thermal, and Fluid Science* 50: 114-126.

Zeitoun, O. 2012. Heat transfer between a vertical water jet and a horizontal square surface. *Experimental Heat Transfer* 25(3): 206-221.